Springer

Journal of Mechanical Science and Technology 23 (2009) 707~716

Journal of Mechanical Science and Technology

www.springerlink.com/content/1738-494x
DOI 10.1007/s12206-009-0203-0

Numerical simulation on soot deposition process in laminar ethylene diffusion flames under a microgravity condition †

Jae Hyuk Choi[1,*], Junhong Kim[1], SangKyu Choi[1], Byoung-Ho Jeon[2], Osamu Fujita[3] and Suk Ho Chung[1]

[1]*School of Mechanical and Aerospace Engineering, Seoul National University, Seoul, 151-742, Korea*
[2]*Aeropropulsion Department, Korea Aerospace Research Institute, Daejeon, 305-333, Korea*
[3]*Division of Mechanical and Space Engineering Hokkaido University, Sapporo, 060-8628, Japan*

(Manuscript Received March 13, 2008; Revised December 18, 2008; Accepted January 23, 2009)

Abstract

A numerical study on soot deposition in ethylene diffusion flames has been conducted to elucidate the effect of thermophoresis on soot particles under a microgravity environment. Time-dependent reactive-flow Navier-Stokes equations coupled with the modeling of soot formation have been solved. The model was validated by comparing the simulation results with the previous experimental data for a laminar diffusion flame of ethylene (C_2H_4) with enriched oxygen (35% O_2 + 65% N_2) along a solid wall. In particular, the effect of surrounding air velocity as a major calculation parameter has been investigated. Especially, the soot deposition length defined as the transverse travel distance to the wall in the streamwise direction is introduced as a parameter to evaluate the soot deposition tendency on the wall. The calculation result exhibits that there existed an optimal air velocity for the early deposition of soot on the surface, which was in good agreement with the previous experimental results. The reason has been attributed to the balance between the effects of the thermophoretic force and convective motion.

Keywords: Diffusion flame; Soot deposition length; Thermophoresis; Microgravity

1. Introduction

Soot particles generated in flames play an important role as a heat radiating medium which can be desirable soot radiation in improving thermal efficiency in large-scale boilers of furnaces, while soot is a common air pollutant and soot deposition on heat exchangers may cause significant deterioration of thermal efficiency [1]. Therefore, the effective control of soot deposition and formation processes is an interesting subject in combustion fields. The characteristics of the soot deposition process form one of the key subjects in preheated air combustion for industrial application. However, information available on these processes is rather limited.

A common example of soot deposition is the blackening of the glass globe of a kerosene lantern; the temperature gradient established between the flame and the globe drives the carbon particles produced in the combustion process towards the globe, where they deposit. For particle adhesion to a wall with a temperature gradient, it is known that the thermophoretic effect is a dominating factor [2]. Deposition by thermophoresis is of considerable practical importance in many industrial applications when hot gases containing small suspended particles flow over cold surfaces [3, 4].

Previous studies on thermophoretic effect induced by temperature gradient have focused on the thermophoretic effect on aerosols or tracer particles in gases or liquids [5-10]. Adomeit et al. [6] performed experiments and numerical simulations on the deposi-

† This paper was recommended for publication in revised form by Associate Editor Ohchae Kwon

*Corresponding author. Tel.: +82 2 880 1706, Fax.: +82 2 889 1842
E-mail address: jhhair@hanmail.net

tion of small particles from turbulent liquid flow and indicated that thermophoresis enhances the particle deposition on cold surfaces. Kang et al. [8, 9] conducted numerical calculation on the thermophoretic particle deposition in the outside vapor deposition (OVD) process. Choi et al. [10] performed a study on particle deposition considering thermophoresis during the OVD process and indicated that as the flow rate of carrier gas increased, the efficiency decreased due to the increase in surface temperature, while the deposition rate increased. Although these studies elucidate the importance of thermophoretic effect, the thermophoretic effect acting on soot particles in flames could behave differently because of particle morphology and chemical components of particles. Considering the thermophoretic effect acting on soot particles, Rosner et al. [11] conducted theoretical research and indicated that the thermophoresis effect on soot particles was insensitive to sizes and morphologies of aggregates. However, the studies on the thermophoresis effect on soot generated in actual flames are very limited, because they are strongly influenced by natural convection such that the identification of the thermophoretic effect on soot is rather difficult.

Recently, several experiments have been performed under a microgravity condition to obtain data on the behavior of soot particles in the field with temperature gradient [12-14]. Choi et al. [15-17] have carried out the in-situ observations of soot particle deposition process in laminar diffusion flames in microgravity condition. In particular, an experimental study to investigate the effect of thermophoresis on soot particles in laminar flames with various surrounding air velocities has been performed [17]. The results showed that there existed an optimal air velocity for the enhanced deposition of soot on the surface.

To clarify the effect of thermophoresis and existence of an optimal air velocity on soot deposition in laminar flames for various surrounding air velocities, the present study analyzed numerically the soot behavior in laminar diffusion flames along a solid wall. Through the simulation, the importance of the thermophoretic effect can be identified and the reason for the optimal velocity for soot deposition can be successfully explained. In addition, the soot deposition length defined as the transverse travel distance to the wall in the streamwise direction is introduced as a parameter to evaluate the soot deposition tendency on the wall.

2. Numerical simulation

2.1 Governing equations

The numerical simulation solved the two-dimensional, time-dependent, and reactive-flow governing equations of the continuity, momentum, species, and energy [18] in axisymmetric coordinates (x, z). The gravitational term is excluded in the momentum equation. The governing equations include terms for convection, thermal conduction, molecular diffusion, viscosity, chemical reaction and radiation transport. The energy equation includes radiative effects from soot, CO_2, and H_2O [19-21]. The radiation transport model adopts the optically thin assumption of

$$-\nabla \cdot q_r = 4a_{overall}\sigma(T^4 - T_\infty^4) \tag{1}$$

where q_r is heat radiative flux, σ is the Stefan-Boltzmann constant, and $a_{overall}$ is the overall Planck mean absorption coefficient.

The absorption coefficient for soot is based on the experiment data of Kent and Honnery [19] and the absorption coefficient for the mixture of CO_2 and H_2O is from the experiment and theoretical work of Magnussen and Hjertager [20]. The overall absorption coefficient for each cell for the sum of soot and the mixture of CO_2 and H_2O was calculated [21].

In the experimental results [17], the soot between flame and wall becomes concentrated at a specific transverse position as z increases. To demonstrate the phenomenon, in this study, the soot number density and the soot volume fraction were calculated. The following soot conservation equations were proposed by Moss et al. [22] based on their experimental results in ethylene-air nonpremixed flames and included source terms for soot nucleation, surface growth, coagulation, and oxidation:

Soot number density

$$\frac{\partial n}{\partial t} + \nabla \cdot (n\mathbf{u}) = -\nabla \cdot (v_{t,x_i} n) + \omega_n \tag{2}$$

Soot volume fraction

$$\frac{\partial f_v}{\partial t} + \nabla \cdot (f_v \mathbf{u}) = -\nabla \cdot (v_{t,x_i} f_v) + \omega_{f_v} \tag{3}$$

where n is the soot number density, f_v is the soot volume fraction and $v_{t,xi}$ is the thermophoretic velocity of soot. Here, ω_n and ω_{fv} indicate the source terms in soot number density, n, and soot volume fraction, f_v,

respectively.

These soot conservation equations also include terms for convection and thermophoresis. The thermophoretic velocity was adopted from the Waldmann formula [23], defined as

$$v_{t,x_i} = -0.54 \cdot \frac{\mu}{\rho} \cdot \frac{\nabla T}{T} \quad x_i = x, z \tag{4}$$

where ρ is the density, μ is the dynamic viscosity, ∇T is the temperature gradient, and T is the temperature. The effect of thermophoresis has been considered in both x and z directions.

The source terms of ω_n and ω_{fv}, in Eqs. 2 and 3 include terms for soot nucleation, surface growth, coagulation, and oxidation [21]:

$$\omega_n = C_\alpha N_o \rho^2 T^{1/2} X_{fuel} e^{-T_\alpha/T} - \frac{C_\beta}{N_o} T^{1/2} n^2 \tag{5}$$

$$\omega_{f_v} = \frac{C_\delta}{\rho_{soot}} C_\alpha \rho^2 T^{1/2} X_{fuel} e^{-T_\alpha/T} + \frac{C_\gamma}{\rho_{soot}} \rho T^{1/2} X_{fuel} e^{-T_\gamma/T} n - \frac{(36\pi)^{1/3} W_{ox} n^{1/3} f_v^{2/3}}{\rho_{soot}} \tag{6}$$

where the soot particle density ρ_{soot} is assumed to be 1.8 g/cm^3, N_o is Avogadro's number, W_{ox} is the Nagle-Strickland-Constable oxidation rate [24] by O_2, T_α and T_γ are the activation temperatures, X_{fuel} is the mole fraction of a fuel and $C_{\alpha,\beta,\gamma,\delta}$ are prescribed numerical constants. And ρ and T are the local mixture density and temperature, respectively. The terms on the RHS of Eq. (5) correspond to the nucleation and coagulation, while the terms on the RHS of Eq. (6) represent the nucleation, surface growth, and oxidation. The values of $C_{\alpha,\beta,\gamma,\delta}$ and the activation temperatures T_α and T_γ are from Refs. [21, 22] as $C_\alpha = 1.7\times10^8 \text{cm}^3/(\text{g}^2\text{K}^{1/2}\text{s})$, $C_\beta = 1\times10^{15} \text{cm}^3/(\text{K}^{1/2}\text{s})$, $C_\gamma = 4.2\times10^{-11} \text{cm}^3/(\text{K}^{1/2}\text{s})$, $C_\delta = 144\times10^3 \text{g}$, $T_\alpha = 46.1\times10^3 \text{K}$, and $T_\gamma = 12.6\times10^3 \text{K}$.

2.2 Numerical method

The calculations were based on a direct numerical simulation (DNS) code with a low Mach number approximation [25], so that the zero-order pressure term was constant over the computational domain and the first-order term was governed by the Poisson equation. A finite difference procedure on a staggered grid was adopted by using a second-order central difference scheme. The second-order predictor-corrector scheme used was a time integration algorithm [26]. A uniform grid system was applied. The Poisson equation could not be solved directly with the spectral method; instead, the multigrid method was used in the axial direction as a fast iterative method. In the radial direction, the Poisson solver adapted the tridiagonal matrix solver (TDMA). A simple one-step chemistry model was adopted by considering variables of the heat of reaction and the activation temperature for laminar ethylene nonpremixed flame [27]. The one step model may limit detailed explanations of the flame structure; however, the hydrodynamic and thermal fields can be reasonably well described. Thermodynamic and transport properties were evaluated with CHEMKIN-III [28] and the Transport Package [29].

As shown in Fig. 1, an axisymmetric cylindrical rod-burner was used in the experiment. The detailed explanation was described previously [15-17]. In the present calculation, an axisymmetric coordinate system was adopted to compare the experiment with the calculation. Fig. 2 shows the schematic of the compu-

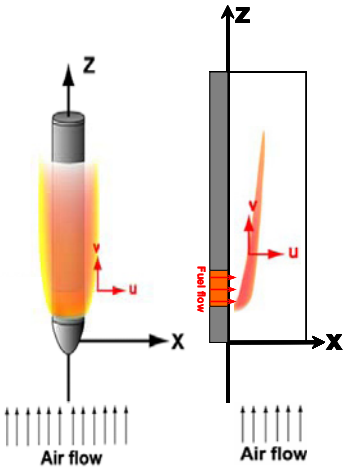

Fig. 1. Schematic of experiment and calculation model.

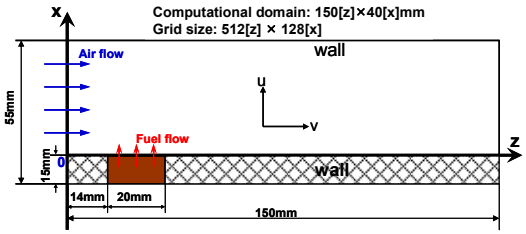

Fig. 2. Schematic of computational domain.

tational domain. In the radial and axial directions, the computational domain was 150(x)× 40 mm(z) mm with 512 ×128 meshes having the mesh sizes of 0.29 and 0.31 mm, respectively. The time step was 5μs and the thermodynamic pressure was assumed to be constant. To match the experimental conditions [17], the fuel velocity with 0.8 cm/s was ejected in the region of z = 14 - 34 mm and the profile of the fuel exit velocity was modeled as a uniform flow. The air velocities were 2.5, 5, and 10 cm/s, and a uniform velocity profile was assumed for the inlet condition. The wall temperature of the burner from z = 34 mm was set at 300 K. At the outlet, all scalar variables and velocity vectors were evaluated from the convective boundary conditions [25]. At the wall, zero fluxes of the scalar variables and normal velocities were applied.

3. Results and discussion

The soot deposition process in laminar diffusion flame along a solid wall under a microgravity condition simulated in this study has been previously investigated experimentally [17]. An ethylene (C_2H_4) diffusion flame was formed around a cylindrical rod-burner with the air velocities of V_a = 2.5, 5, and 10 cm/s. The experimental result showed that the region of the soot particle distribution moved closer to the burner wall as the surrounding air velocity increased. Because of the simultaneous effects of convection and the thermophoresis, soot particles finally adhered to the burner wall. Moreover, the soot locus for V_a = 5 cm/s was shorter than that of V_a = 2.5 and 10 cm/s. It implied that there existed an optimal air velocity for the early deposition of soot on the surface due to variations in the velocity field and in the temperature field by the change in the air velocity. Thus, a numerical analysis was conducted to better understand the behavior of soot deposition in the laminar diffusion flame near a solid wall at various air velocities.

Fig. 3 shows the distribution of temperature and the reaction rate at various air velocities (V_a =2.5, 5 and 10 cm/s). Here, x is the coordinate denoting the vertical distance from the burner surface. For the calculation, the wall temperature and fuel jet velocity were fixed at Tw = 300 K and Uf = 0.8 cm/s, respectively. The contour of the temperature distribution in Fig. 3(a) shows a good agreement with the observed flame shape in Ref. 17. As shown in Ref. 17, the flame luminosity with V_a = 10 cm/s was brighter than that of the other flames. The differences in flame luminosity

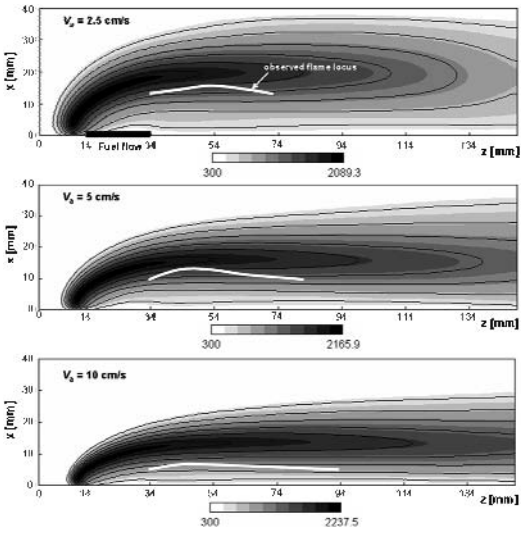

(a) Distribution of temperature

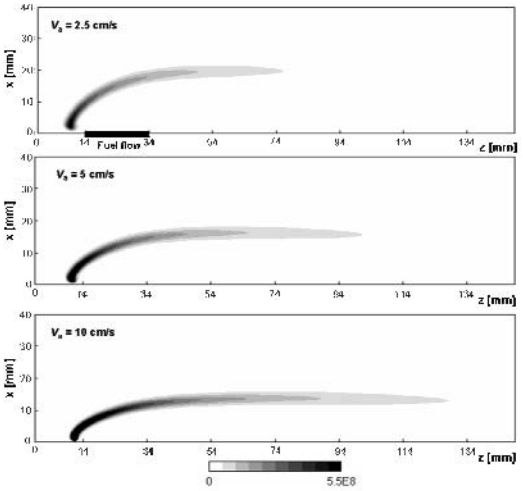

(b) Distribution of reaction rate

Fig. 3. Distributions of temperature (a) and reaction rate (b) at various air velocities.

suggest substantial changes in temperature. The calculated maximum temperatures were 2089 K for V_a = 2.5 cm/s, 2165 K for V_a = 5 cm/s, and 2237 K for V_a = 10 cm/s. The increasing temperature with increased air velocity is consistent with the behavior of the observed flame luminosity.

In Fig. 3(a), the solids lines are observed flame loci. The observed flame locus corresponding to the outer edge of the visible flame was located a few mm inside of the maximum temperature position. This can be explained from the fact that the visible flame is the

result of incandescent soot and it usually appears on the fuel side rather than along the reaction zone, that is, along the maximum temperature position. It can also be observed in Fig. 3(a) that the temperature contours for V_a = 10 cm/s elongate further downstream as compared to the cases for V_a = 2.5 and 5 cm/s. The contour of the reaction rate in Fig. 3(b) further substantiates this behavior. Simultaneously, the contour of the reaction rate moves to the wall with increasing air velocity, which also agrees with the phenomena observed in Ref. 17. The length of the reaction zone increases with the air velocity, which agrees well with the observation in Ref. 17. These qualitative results compared to the experimental data show similar flame shapes and overall flame height from burner wall.

In the experiment [17], soot particles for the three cases were deposited on the wall around z = 104 mm (90 mm from the front end of the fuel injection). Thus, in this study, the results are analyzed at z = 104 mm. Figure 4 shows the distribution of temperature at z = 104 mm based on the results in Fig. 3. The maximum temperature increases with the increase in the air velocity. When the air velocity is 10 cm/s, the position of the maximum temperature is much closer to the wall than those at 2.5 and 5 cm/s. The appreciable change in the position of the maximum temperature with the air velocity can be explained by the fact that the increased air velocity makes the fuel stream to approach nearer to the wall. Consequently, the stoichiometric contour, an indication of the diffusion flame, shifts towards the burner wall. A notable feature is that the differences in the temperature by the change in the air velocity mitigate very near the wall. This implies that the difference in thermophoretic velocity caused by temperature gradient very near the wall would also be small.

Fig. 5 shows the distribution of the v-velocity at z = 104 mm. The values of v-velocities increase with increasing air velocity. The maximum velocities at various air velocities appear around x = 12-15 mm. The maximum velocities are 33.03 and 11.03 cm/s at V_a = 10 and 2.5 cm/s, respectively. The maximum velocity at V_a = 10 cm/s is about 3 times higher than that of V_a = 2.5 cm/s. The differences of the velocities near the wall are appreciable. This suggests that the effect of v-velocity in the axial direction near the surface of the wall is expected to be large. This also implies that the residence time of the soot particles near the wall could be influenced by the air velocity. It is thought that the residence time of soot particles becomes short and the deposition of soot particles on the wall is delayed as the air velocity increases. Therefore, when the air velocity is 10 cm/s, soot particles will move downstream fastest through the combustion zone due to relatively shorter residence time due to high v-velocity in the axial direction, resulting in the position of soot deposition further away from the fuel injection zone. As the air velocity decreases, while the residence time of soot particles becomes relatively longer, the distance between flame and wall is much broader than that of other cases, as was shown in Fig. 3. As a consequence, soot particles have enough time to flow to lower position of the burner and the position of soot deposition is far from a burner exit.

Fig. 6 shows the profiles of the thermophoretic velocity U_t, the gas velocity Ug, and the particle velocity $U_p = U_g + U_t$ in the transverse x-direction at z = 104 mm, where the thermophoretic velocity was calculated

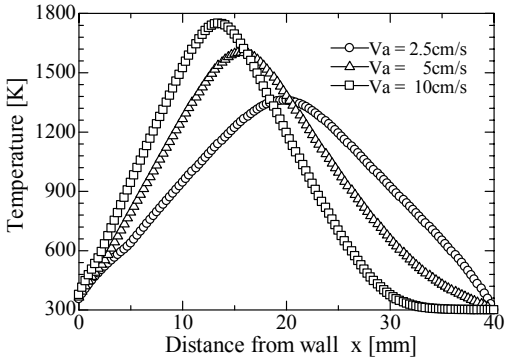

Fig. 4. Temperature distribution at various air velocities (z = 104 mm).

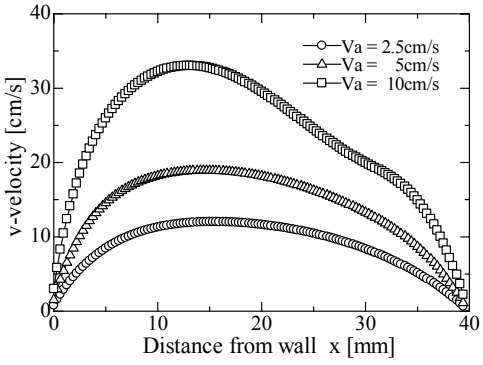

Fig. 5. Profiles of v-velocity in the streamwise direction at various air velocities (z = 104 mm).

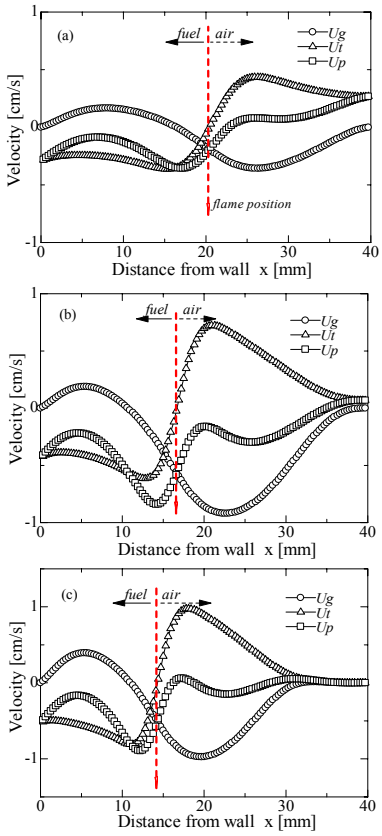

Fig. 6. Profiles of thermophoretic velocity Ut , transverse gas velocity Ug, and particle velocity Up along radial direction at z = 104mm : (a) Va = 2.5cm/s, (b) 5 cm/s and (c) 10 cm/s.

from Eq. (4). The gas velocity Ug on the air side has negative values, while has positive values on the fuel side. In general, U_g is expected to have positive values in an open domain because of the expansion of gas in a flame zone. The present negative value can be attributed to the effect of confinement by the top lid of the duct.

The gas velocities U_g at the wall vanish by the non-permeable wall condition at z = 104 mm. The variation near the wall, for example, x < 1 mm, is very small for all the air velocity conditions. The particle velocities at x = 1 mm are – 0.25, – 0.42, and – 0.47 cm/s at Va = 2.5, 5.0 and 10 cm/s, respectively. This indicates that the particle velocity is almost exclusively determined by the thermophoretic velocity near the wall and, thus, the thermophoretic force is the dominant factor in soot motion. Note that the thermophoretic velocity U_t , becomes nearly zero near the flame position, where the temperature is maximum; thus the temperature gradient is zero. The particle velocity in the flame zone is controlled by the gas velocity, implying that the gas expansion is the dominant controlling parameter in soot motion near the flame zone.

An interesting feature is that the difference in the thermophoretic velocity between V_a = 5 cm/s and 10 cm/s is not large. While, in Fig. 5, the streamwise v-velocity for V_a = 10 cm/s is twice larger than that for V_a = 5 cm/s near the wall. Based on these behaviors, the deposition of soot on the wall for V_a = 5 cm/s is easier than for V_a = 10 cm/s.

It is an important factor whether soot particles can reach the wall during the residence time of soot particles in the flow field. In this regard, the soot deposition length (L_{soot}), which is defined as the transverse travel distance to the wall in the streamwise direction, is introduced as a parameter to evaluate the soot deposition tendency on the wall:

$$L_{soot} = -U_P \times \tau_{soot} \tag{7}$$

$$\tau_f = L_C \times |V_P| \tag{8}$$

where L_c is the characteristic length (135mm in this study) , V_p is the particle velocity in z-direction and U_p is the particle velocity in x-direction. Here, τf can be regarded as the residence time of soot particles inside flame.

Fig. 7 shows the distribution of soot deposition length, L_{soot}, without and with considering the thermophoretic velocity at various air velocities for z = 104 mm. L_{soot} has been calculated with Eq. (7). Without considering the thermophoretic velocity (a), L_{soot} near the surface of the wall at three velocities (V_a = 2.5, 5 and 10 cm/s) has negative values. Physically, this means that it is difficult for soot to be deposited on the wall. On the other hand, with considering thermophoretic velocity (b), all values of L_{soot} near the wall have positive values. This implies that soot particles can be deposited on the surface of the wall. An interesting feature is that the relatively high soot deposition lengths are maintained between x =1 mm and x =15 mm when the surrounding air velocity is V_a = 5 cm/s. This means that soot particles could be easier to be deposited on the wall.

Fig. 8 shows the distributions of the soot deposition length of radial locations at different distances (z) from the point of gas injection at various air velocities. The result shows that L_{soot} at V_a = 5 cm/s is higher than that of V_a = 2.5 and 10 cm/s at each z position.

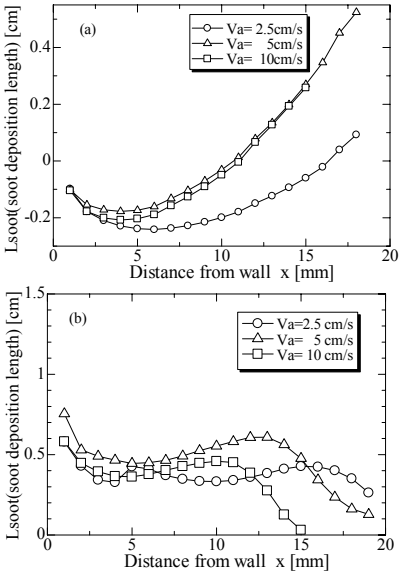

Fig. 7. Soot Deposition length distribution (a) without considering thermophoretic velocity and (b) with considering thermophoretic velocity for various oxidizer velocities at z = 104 mm.

Especially, the values of L_{soot} near the surface of the wall at z = 84, 104, 124 mm are high. This indicates that it is much easier for soot particles to be deposited on the wall and the amount of soot particles on the wall would be enhanced as soot particles move downstream.

From the results in Figs. 3-8, as the air velocity increases, the thermophoretic velocity increases with the increase in the air velocity because the fuel stream approaches near the wall. While, the temperature variations in flame according to the air velocities are small, as shown in Fig. 3(a). Therefore, the difference of thermophoretic velocity in flame is small. On the other hand, the volumetric velocity in flame is increased considerably as air velocity increases. Therefore, even though the thermophoretic velocity near the surface of the wall for V_a = 10 cm/s has a slightly higher value, due to relatively high velocity in the z direction, the L_{soot} for V_a = 10 cm/s is expected to be smaller than that for V_a = 5 cm/s. When the air velocity is V_a = 2.5 cm/s, as shown in Fig. 3, the flame temperature and the distance between flame and the surface of wall are smaller and broader than those for V_a = 5 cm/s. This means that soot particles have enough time to flow to lower position from the burner exit, and the temperature very near the burner wall would be decreased as it goes to lower position of

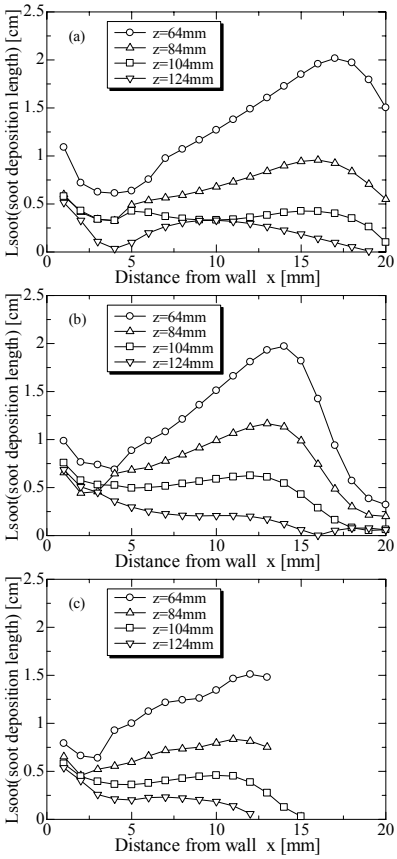

Fig. 8. Predicted soot deposition length at different distances (z) from the fuel inlet: (a) Va = 2.5cm/s, (b) Va = 5 cm/s and (c)Va = 10 cm/s.

burner. Therefore, the thermophoretic velocity caused by the temperature gradient is also decreased. As a result, L_{soot} for V_a = 2.5 cm/s can be smaller than that for V_a = 5 cm/s because of longer distance between the flame and the wall as well as relatively small thermophoretic velocity near the wall.

As mentioned above, in the previous work [17], the values of maximum soot volume fractions at V_a = 5 cm/s were increased with increasing z; 3.83 ×10-6 at z = 64 mm, 4.39 ×10-6 at z = 84 mm, 5.11 ×10-6 at z = 104 mm and 5.86 ×10-6 at z = 124 mm. This trend was explained as "widely distributed soot between flame and wall concentrates on a certain streamwise position". This trend was also showed at V_a = 2.5 and 10 cm/s. Thus, in the present study, a numerical calculation was conducted to demonstrate the trend.

Fig. 9 shows the profiles of the calculated soot volume fractions as a function of transverse coordinate for z = 64, 84, 104, and 124mm at various air veloci-

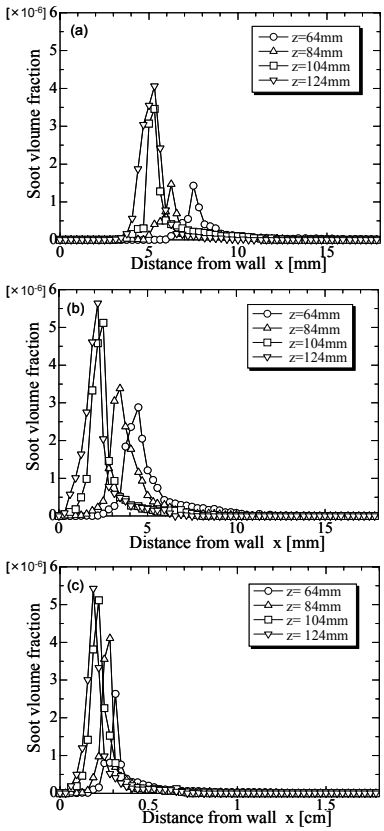

Fig. 9. Predicted soot volume fractions at different distances (z) from the fuel inlet: (a) Va = 2.5cm/s, (b) Va = 5 cm/s and (c)Va = 10 cm/s.

ties. Note that the conservation equations for the soot number density and volume fraction include terms for convection, thermophoresis, and source terms. The thermophoresis terms in the x- and z-directions were considered. The source terms include terms for soot nucleation, surface growth, coagulation, and oxidation. In Fig. 9, the values of the calculated maximum soot volume fraction at V_a = 5 cm/s increase with increase in z; 2.88 ×10-6 at z = 64 mm, 3.38 ×10-6 at z = 84 mm, 5.12 ×10-6 at z = 104 mm and 5.54 ×10-6 at z = 124 mm. The positions of maximum soot volume fractions for V_a = 2.5cm/s are the farthest from the wall at various air velocities. This result implies that the amount of soot deposited on a solid wall can be decreased. In Fig. 9, although the soot region in the flame is narrower and the quantity of soot is considerably reduced very near the wall (for x < 3 mm), the overall behavior of the calculated maximum soot locus is similar to that of the experiment results [17], moving close to the wall as the velocity increases.

4. Concluding remarks

Characteristics of soot behavior and soot deposition on the surface of the wall in laminar diffusion flames along the solid wall for various surrounding air velocities under a microgravity condition have been analyzed numerically, accounting for the thermophoretic effect. Especially, the soot deposition length (L_{soot}) defined as the relative approach distance to the wall per a given axial distance is introduced as a parameter to evaluate the soot deposition tendency on the wall. The numerical results show that the values of Lsoot near the surface of the wall at various air velocities (V_a = 2.5, 5 and 10 cm/s) show negative values without considering thermophoretic velocity. On the other hand, with considering thermophoretic velocity, all values of Lsoot near the surface of the wall have positive values. The results demonstrate that a consideration of thermophoresis is essential to estimate the behavior of soot deposition on the walls. When the surrounding air velocity was beyond a critical velocity, V_a = 10 cm/s, the soot deposition length was diminished due to the relatively fast v-velocity in the axial direction, resulting in soot deposition on the surface of the wall becoming difficult. The relatively high soot deposition length at V_a = 5 cm/s is maintained at all positions in the x-direction at z = 104 mm, indicating that it is easier for soot particles to be deposited on the wall and the amount of soot particles on the wall would be enhanced.

The numerical analysis successfully predicted that there existed an optimal air velocity for the early deposition of soot on the surface of the wall, and the thermophoretic velocity plays an important role in the soot deposition on the wall.

Acknowledgment

This work was sponsored by CERC and JHC was supported by the Brain Korea 21 project.

References

[1] N. Montassier, D. Bouloud and A. Renoux, Experimental study of thermophoretic particle deposition in laminar tube, J. of Aerosol Sci., 22 (1991) 677-687.

[2] L. Talbot, R. K. Cheng, R. W. Schefer and D. R. Willis, Thermophoresis of particles in a heated boundary layer, J. of Fluid Mech. 101 (1980) 737-758.

[3] G. K. Batchelor and C. Shen, Thermophoretic deposition of particles in gas flowing over cold surfaces, J. of Colloid Interface Sci. 107 (1985) 21-37.

[4] A. G. B. M. Sasse, W. W. Nazaroff and A. J. Gadgil, Particle filter based on thermophoresis deposition from natural convection flow, Aerosol Sci. Tech. 20 (1980) 227-238.

[5] C. J. Sun, C. K. Law and R. L. Axelbaum, Thermophoretic effects on seeding particles in LDV measurements of strained flames, Combust. and Flame, 105 (1994) 189-201.

[6] P. Adomeit and U. Renz, Deposition of fine particles from a turbulent liquid flow: Experiments and Numerical Predictions, Chem. Eng. Sci., 51 (13) (1996) 3491-3503.

[7] R. Tsai and L. J. Liang, Correlation for thermophoretic deposition of aerosol particles onto cold plate, J. of Aerosol Sci., 32 (2001) 473-487.

[8] S. H. Kang and R. Grief, Thermophoretic transport in the outside vapor deposition process, Int. J. of Heat and Mass Transfer, 36 (1993) 1007-1018.

[9] S. H. Kang and K. H. Hong, Three dimensional analysis of the thermophoretic particle deposition in OVD (Outside Vapor Deposition) Process, Proc. of the 3rd KSME-JSME, (1996) Ⅱ-71-Ⅱ-76.

[10] J. Cho, J. Kim and M. Choi, An Experimental study of heat transfer and particle deposition during the outside vapor deposition process, Int. J. of Heat and Mass Transfer, 41 (1998) 435-445.

[11] D. E. Rosner, D. W. Mackowski and Garcia-Ybarra., Size and structure-Insensitivity of the thermophoretic transport of aggregated soot particle in gases, Combust. Sci. Tech., 80 (1991) 87-101.

[12] O. Fujita and Y. Takeshita, Effect of Thermophoretic force on soot agglomeration process in diffusion flames under microgravity, the 4th International Microgravity combustion Workshop, NASACP 10194, (1997) 217-222.

[13] A. Toda, H. Ohi, R. Dobashi, T. Hirano and T. Sakuraya, Accurate measurement of thermophoretic effect in microgravity, J. of Chem. and Physics,105 (16) (1996) 7083-7087.

[14] H. Ono, R. Dobashi and T. Sakuraya , Thermophoretic velocity measurement of soot particles under a microgravity condition, Proc. Combust. Institute 29, (2002) 2375-2382.

[15] J. H. Choi, O. Fujita, T. Tsuiki, J. Kim and S. H. Chung, A study of the effect of Oxygen concentration on the soot deposition process in a diffusion flame along a solid wall by in-situ observation in microgravity, JSME(B) Int. J., 48 (4) (2005) 839-848.

[16] J. H. Choi, O. Fujita, T. Tsuiki, J. Kim and S. H. Chung, In-situ observation of the soot deposition process on a solid wall with a diffusion flame along the wall, JSME(B) Int. J., 49 (1) (2006) 167-175.

[17] J. H. Choi, O. Fujita, T. Tsuiki, J. Kim and S. H. Chung, Experimental study on thermophoretic deposition of soot particles in laminar diffusion flames along a solid wall in Microgravity, Experimental Thermal and Fluid Sci., 32 (2008) 1484-1491.

[18] F. A. William, Combustion theory, Second edition, The Benjamin/Cummings Publishing Company (1985).

[19] J. H. Kent and D. R. Honnry, A soot formation rate map for a laminar ethylene diffusion flame, Combust. Flame 79 (1990) 287-298.

[20] B. F. Magnussen and B. H. Hjertager, On mathematical modeling of turbulent combustion with special emphasis on soot formation and combustion, Int. Sixteenth Symp. in Combustion, (1977) 719-729.

[21] C. R. Kaplan, S.W. Baek, E. S. Oran and J.L. Ellsey, Dynamic of a strongly radiating unsteady ethylene jet diffusion flame, Combust. and Flame, 96 (1994) 1-21.

[22] J. B. Moss, C. D. Stewart and K. J. Young, Modeling soot formation and burnout in a high temperature laminar diffusion flame burning under oxygen-enriched conditions, Combust. and Flame, 101 (1995) 491-500.

[23] Waldmann., On the Motion of spherical particles in nonhomogeneous gases, Academic Press Inc., (1961) 323-344.

[24] J. Nagle and R. F. Strickland-Constable, Proc. of Fifth Carbon Conference, 1 (1962) 154-164.

[25] S. Mahalingam, B. J. Cantwell and J. H. Ferziger, Non-premixed combustion: Full numerical simulation of a coflowing axisymmetric Jet, inviscid and viscous stability analysis, report TF-43, Thermoscience Division, Stanford University, Stanford, California, (1989).

[26] H. N. Najm, P. S. Wyckoff and O. M. Kino, J. Compu. Phys. 143, (1998) 381-402.

[27] F. T. Eduardo, L. A. Antonio, L. Amable and F. A. Williams, A simple one -step chemistry model for partially premixed hydrogen combustion, Combust. and Flame, 147 (2006) 32-38.

[28] R. J. Kee, F. M. Rupley, E. Meeks and J. A. Miller, CHEMKIN-III: A Fortran chemical kinetics pack-

age for the analysis of gas-phase chemical and plasma kinetics, SAND96-8216, Sandia National Laboratories, Livermore, CA, (1996).
[29] R. J. Kee, J. Warnatz and J. A. Miller, A Fortran computer code package for the evaluation of gas phase viscosities, conductivities and diffusion coefficients, Sandia report SAND83-8209.

Jae Hyuk Choi received his B.S. and M.S. degrees in Marine System Engineering from Korea Maritime University in 1996 and 2000, respectively. He then went on to receive a Ph.D. degrees from Hokkaido university in 2005. Dr. Choi is currently a BK21 Assistant Professor at the School of Mechanical and Aerospace Engineering at Seoul National University in Seoul, Korea. Dr. Choi's research interests are in the area of reduction of pollutant emission (Soot and NOx), high temperature combustion, laser diagnostics, alternative fuel and hydrogen production with high temperature electrolysis steam (HTES).

Junhong Kim received his B.S., M.S., and Ph. D degrees in Mechanical Engineering from Seoul National University in 1998, 2000, and 2004, respectively. His research interests include lifted flames, edge flames, and numerical simulation.

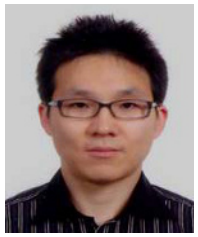

Sang Kyu Choi received his B.S. degree in Mechanical Engineering from Seoul National University in 2004. He is a Ph. D student in the School of Mechanical Engineering, Seoul National University. His research interests include edge flames, oxy-fuel combustion, and numerical simulation.

Byoung ho Jeon received his B.S degrees in Mechanical Engineering from kangwon University in 1998, and M.S., Ph. D. degrees in Mechanical Engineering from Hokkaido University in 2002, 2008, respectively. Dr Jeon is working at Korea Aerospace Research Institute from 2007. June. as Gasturbine engine developer. Jeon's research interests are in the area of reduction of pollutant emission (Soot and Nox), High temperature combustion, combustion system (Furnace, Combine Generation system, IGCC, CTL), and Fire safety in building.

Osamu Fujita received his B.S., M.S., and Ph. D. degrees in Mechanical Engineering from Hokkaido University in 1982, 1984, and 1987, respectively. Prof. Fujita is currently a Professor at the division of Mechanical and space Engineering at Hokkaido University in sapporo, Japan. Prof. Fujita's research interests are in the area of reduction of pollutant emission (Soot and Nox), solid combustion, catalytic combustion, high temperature combustion, alternative fuel and fire safety in space.

Suk Ho Chung received his B.S. degree in Mechanical Engineering in 1976 from Seoul National University, and his M.S. and Ph. D. degree in Mechanical Engineering in 1980 and 1983, respectively from Northwestern University. He is a professor since 1984 in the School of Mechanical and Aerospace Engineering, Seoul National University. His research interests cover combustion fundamentals, pollutant formation, and laser diagnostics.